Journal of Metals, Materials and Minerals, Vol.19 No.2 pp.95-99, 2009.

Burning Temperature Dependence of Rice Husk Ashes in Structure and Property

Liangming XIONG,[1*] Edson H. SEKIYA,[1] Pornapa SUJARIDWORAKUN,[1,2] Shigetaka WADA[2] and Kazuya SAITO[1]

[1]*Frontier Materials Lab, Research Center for Advanced Photon Technology, Toyota Technological Institute, Nagoya, 468-8511, Japan.*
[2]*Department of Materials Science, Chulalongkorn University, Bangkok, 10330, Thailand.*

Abstract

Much attention has been paid to the characterization of the structure and properties of rice husk ash (RHA), but little to the burning temperature dependence of its structure and properties. This dependence is important for the structure and property optimization of RHA in a controllable manner. In this paper, we present a research on the burning temperature dependence of RHA. Rice husk (RH) was burned at various temperatures either as received or after pretreatment by HCl washing. The obtained ashes of both groups exhibit a strong burning temperature dependence of the specific surface area and pore volume, based on the N_2-sorption results. According to the X-ray diffraction (XRD) results, the short range ordered structure of the rice husk silica (RHS) exhibits a decreased densification with the burning temperature; According to the infrared absorption (IR) spectroscopic results, the Si–O–Si angle of RHS was increased with the burning temperature. Based on this dependence, a decreased burning temperature is highly desirable for applications of RHA in catalysis, absorption, and chemical synthesis as Si source.

Key words: Rice husk ash, Burning temperature, Physicochemical property, Infrared absorption, Densification.

Introduction

The production of rice, one of the major food crops in the world, generates one of the major wastes of the world, namely, rice husks (RHs). The abundant, cheap, regenerable RHs naturally have high contents of silica and the silica has a high reactivity.(7) Thus, how to extract highly pure silica from RHs, and make an efficient use of it, has recently received more and more attention.

When RH is combusted in air, the combustibles can be mostly burned off and some solid products are left, which are named rice husk ash (RHA). The predominant component of RHA is silica. When RH is treated in solution before combustion, the complete combustion products are almost only silica, >99 % in mass.(8, 11) The silica is porous and has abundant hydrophilic Si–OH groups, therefore adsorbing much moisture. In some sense, the nature of the silica decides the structure and property of RHA.

RHA can be used in many fields.(3,7) For some applications, like catalysis (Chang, *et al.* 2005), adsorption (Feng, *et al.* 2004), and chemical synthesis using RHA as a starting material (Wang, *et al.* 1998, Xiong, *et al.* 2009), RHAs are needed to generate favorable structure and desirable properties. For example, amorphous structure, high specific surface area (SSA), large pore volume (PV), and high reactivity are very important for such applications. These structures and properties in general can vary by the high temperature process of RHA. Moreover, RHA in essence is the product of the high temperature burning process of RH. In other words, the structure and properties of RHA must to some extent be dependent on the burning temperature (T_b). Furthermore, a good understanding of the burning temperature dependence of RHAs is essential for the structure and property optimization on RHA to fulfill various application needs.

Herein, we present a research on the T_b dependence of the structure and physicochemical

E-mail: lmxiong@toyota-ti.ac.jp

properties of RHAs obtained by burning RH either as received or after pretreatment by HCl washing. The short-range order structure, the Si−O−Si bond angle and densification of the amorphous silica, and the SSA and the PV of RHAs were all found depending on T_b.

Materials and Experimental Procedures

The as-received RHs were thoroughly washed with tap water, and then washed with distilled water 3 times by strong stirring. The water-washed husks were dried at 110°C overnight. Next, 100 g of the dried husks were immersed in 2 L of 1 M HCl solution and stirred for 1 hour. The husks were filtered and washed with distilled water 3 times and finally dried at 110°C overnight for subsequent use. The HCl-washed RHs were then burned at 400, 500, 600, 700, 800, and 900°C, respectively, for 2 hours at a heating rate of 10°C min^{-1}. For comparison, some other raw RHs were also burned under the same conditions as the above. Thus, two groups of ash samples were obtained. One was from the raw RHs and the other was from the washed RHs. They are labelled as *r*RHA and *w*RHA, respectively. Finally, all the as-prepared ash samples were further annealed at 900 and 1000°C, respectively.

The wide-angle powder X-ray diffraction (XRD) patterns of the ash samples were taken on a Rigaku RINT-2500 X-ray diffractometer with Mo–K_α (λ = 0.7093 Å) radiation. The Fourier transform infrared (FT-IR) absorption spectrometry was performed on a PerkinElmer Multiscope FT-IR Microscope. The spectrometry was taken in the IR reflection mode, in which the ash sample was directly pressed to form a pellet without addition of KBr. N_2 sorption isotherms were obtained on a Micromiritics Tristar 3000 analyzer at 77.35 K. The surface area and the pore volume were calculated by the Brunauer–Emmett–Teller (BET) theory and the Barrett-Joyner-Halenda (BJH) theory, repectively.

Results and Discussion

Figure 1 shows the XRD results of the ash samples, obtained at various T_b. For *r*RHA, as shown in Figure 1(a), when T_b < 900°C, only the broad amorphous diffractions were collected on the

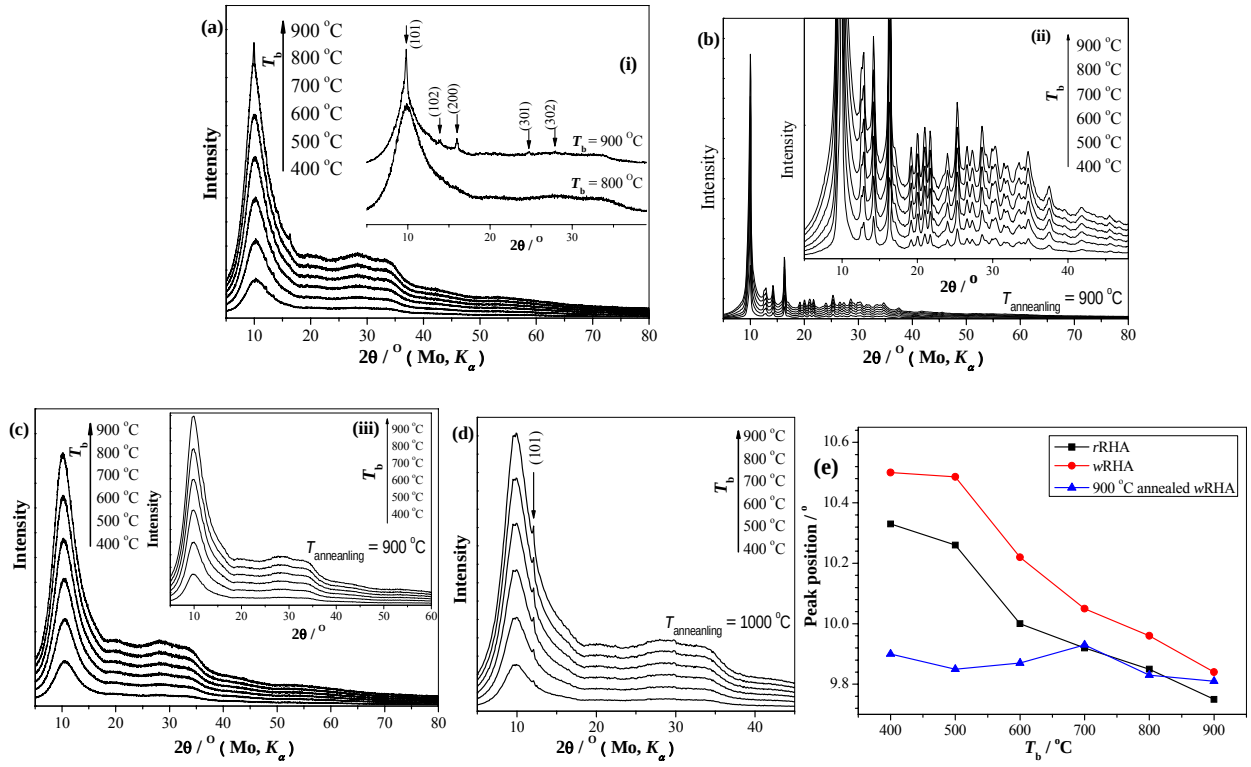

Figure 1. XRD patterns of the ashes: (a) *r*RHAs obtained by burning at various T_b and (b) their corresponding products by annealing at 900°C; (c) *w*RHAs obtained by burning at various T_b and (d) their corresponding products by annealing at 1000°C. Insets: (i) enlarged patterns of *r*RHAs obtained by burning at 800 and 900°C, respectively, in (a); (ii) enlarged XRD patterns in (b); (iii) XRD patterns of the corresponding products after annealing *w*RHAs at 900°C in (c). (e) amorphous peak positions of *r*RHA, *w*RHA, and the 900°C−annealed *w*RHA *vs* T_b.

ashes; when T_b = 900°C, besides the amorphous peaks, some sharp diffraction peaks were clearly exhibited on the ash, as shown in Inset (i). This indicates that some crystallites have been formed at 900°C in the raw husk combustion. The calculated *d*-spacings of the crystal phase can well match those of the pattern collected in JCPDS Cards No. 82-0512, which is one of the standard patterns of cristobalite. Thus, the detected crystal phase is cristobalite. When annealed at 900°C for 2 hours in the same way, all the *r*RHAs were crystallized and exhibited the same crystal diffractions, as shown in Figure 1(b) and Inset (ii). These are the diffractions of crystobalite, according to the above JCPDS card. For *w*RHA, however, no crystal was collected, only the amorphous diffractions were even when T_b = 900°C, as shown in Figure 1(c). This means that some leached-out ions from the husks have favored the crystallization of *r*RHA. The K content was generally recognized to be responsible for this.[6] Moreover, when annealed at 900°C in the same way as *r*RHA, none of the *w*RHA exhibited any crystal diffraction either, as shown in Inset (iii). When the annealing T was increased to 1000°C, a clear sharp diffraction peak occurred at the 2θ= 12.1° position, as shown in Figure 1(d). This diffraction matches the strongest diffraction plane (101) of quartz to a greater extent than other planes or other crystals. Thus, *w*RHA began to be crystallized at 1000°C, forming quartz.

For the non-crystallized ashes, the broad amorphous diffraction is decided by the short range order structure of the amorphous SiO_2. Comparing the strongest amorphous peak positions, the 2θ values of both *r*RHAs and *w*RHAs were found to decrease with the increase of T_b, as shown in Figure 1(e). According to the Bragg Equation ($2d\sin\theta = n\lambda$), a decrease of θ suggests an increase of the d spacing. Thus, the 2θ value decrease with T_b indicates that the short-range order structure blocks became larger with increasing T_b. That illustrates that the densification of the amorphous structure was decreased with T_b. Furthermore, when obtained at the same T_b, the amorphous diffraction peak of *r*RHAs is at a smaller 2θ value compared with *w*RHAs. This also suggests that the amorphous SiO_2 in *r*RHAs has lower densification than that in *w*RHAs. In addition, when *w*RHAs were annealed at 900°C, the position of the strongest amorphous peaks was found close to that of the non-annealed *w*RHA obtained at 900°C, varying little from ash to ash obtained at various T_b.

Among the IR absorption bands of amorphous SiO_2, the band at ~1100 cm^{-1} is the most prominent and occurs with a prominent shoulder at ~1200 cm^{-1}. This band has been directly correlated with the structure and various physical properties of SiO_2 glass.[1] This band is also correlated with Si−O−Si bond angle.[1] It has been found to shift to higher frequencies with increasing the Si−O−Si bond angle. It has also been observed to shift to lower frequencies with increasing densification. Figure 2 shows the change of the 1100 cm^{-1} IR absorption bands of *r*RHA and *w*RHA versus T_b (K). The band of the *r*RHA group shifts to higher frequencies with increasing T_b. This also applies for the band of the *w*RHA group. At the same T_b, the band of *r*RHA peaks at a higher frequency compared with that of *w*RHA. The change in peak positions should reflect a change in the structure of SiO_2 due to a change in T_b or the acid washing pretreatment. According to the previous observations (Agarwal, *et al.* 1995), the T_b dependence of the IR peak position suggests that with increasing T_b in 673 – 1173 K, either the Si−O−Si bond angle of *r*RHA and *w*RHA increases or the densification decreases. This is in obvious agreement with the XRD result above. The higher IR peak position of *r*RHA also suggests that the Si−O−Si bond angle of SiO_2 in *r*RHA is larger or the densification is lower, compared with those of *w*RHA. This is also in positive agreement with the XRD result. A generic line is constructed using a linear regression fit to all of the datapoints. The equations for the *r*RHA and *w*RHA lines in Figure 2 are, respectively,

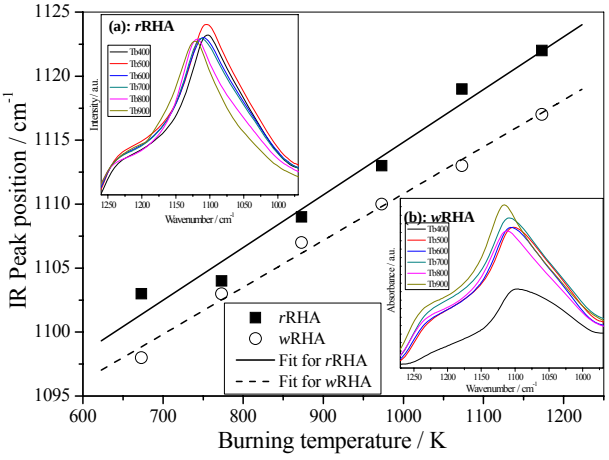

Figure 2. Peak position of IR stretching vibration band of SiO_2 *vs* T_b. Insets: the IR absorption spectra of *r*RHA (a) and *w*RHA (b).

$$\nu_{p\text{-}r} = (1073.692 \pm 2.99) + (0.041 \pm 0.003)*T_b \quad (1)$$

and

$$\nu_{p\text{-}w} = (1074.245 \pm 1.564) + (0.037 \pm 0.002)*T_b, \quad (2)$$

where ν_i (cm^{-1}) is the peak position of the respective bands of *r*RHA and *w*RHA, and T_b (K) is the burning temperature. Taking the measurement and fit errors into account, both lines can be considered parallel with the same slope, which suggests T_b influencing the structure of *r*RHA and *w*RHA in the same manner. Thus, the burning temperatures of the as-received *r*RHA or *w*RHA can be determined from Eqs. (1) or (2) by simply measuring their IR absorption peak positions.

Figure 3 shows the surface area and the pore volume of *r*RHAs and *w*RHAs versus T_b. Evidently, the SSA and the PV of *r*RHAs decreases with the increase of T_b in the range of 400 – 900°C. When T_b reached 800 – 900°C, the SSA was sharply decreased, and the PV was also decreased significantly. A similar case occurred on *r*RHAs, but the maximal surface area, ~235 m^2 g^{-1}, and the maximal pore volume, ~0.32 cm^3 g^{-1}, both occurred at 500°C. Moreover, when T_b reached 800 – 900°C, both the SSA and the PV did not decrease as much as those of *r*RHAs. This T_b dependence of physicochemical properties of both groups of ashes can be explained by a thermal destruction theory. In this theory, porous silica with high SSA has abundant Si–OH groups on the framework surface. As *T* increases, the adjacent Si–OH groups can be further co-condensed, causing the metastable porous framework to be destructed and even collapse. This thermal destruction behavior has been widely investigated on ordered mesoporous silica. This behavior must occur on RHAs, because their silica can also have many Si–OH groups. However, for *r*RHAs, the thermal destruction mechanism should not be the only main mechanism, especially when T_b reached 800 – 900°C. The dramatic decreases of SSA and PV can also be due to solid state reactions between the active RH silica and different impurities. According to (Armesto, *et al.* 2002), the eutectic mixture $K_2O•4SiO_2$ can be formed with a meting point of 764°C in RH combustion. SiO_2 and P_2O_5 are also ready to form phosphosilicate in the T_b range. Although the K and P contents were found to be the main non-carbonaceous impurities in ashes, according to our recent work (Xiong, *et al.* 2009), the existence of K and P must favor the SSA and PV decreases. On the other hand, according to the above XRD results, *r*RHA has some crystallite at 900°C s. The formation and growth of the crystallites should also be responsible for the dramatic SSA and PV decreases. In essence, the early crystallization of *r*RHA is also due to the existence of the K content. Thus, such impurities as K and P result in the larger decrease with T_b.

Note that the SSA of *w*RHAs is more than twice that of *r*RHAs when obtained at the same T_b. The higher SSA can facilitate O_2 to transfer into the pores to take part in the combustion reactions. Taking into account that the washed RH combustion at 500°C was incomplete, higher SSA (>235 m^2 g^{-1}) and PV (>0.32 cm^3 g^{-1}) are expected to be obtained for *w*RHA at ~570°C, according to another part of our recent work.[10] On the basis of the T_b dependence, it is anticipated that a lower T_b, if high enough to burn out combustibles of RH, will obtain an ash with higher SSA and PV. All things considered, a decreased complete combustion *T* of RH is highly desirable for the preparation of high-quality RHA or silica with high SSA and PV, which are particular important for use in catalysis, adsorption, chemical synthesis, and so on. This may be realized by catalytic combustion routes. Recently, we proposed a new catalytic route in which the complete combustion temperature can be decreased by more than 100°C.[10]

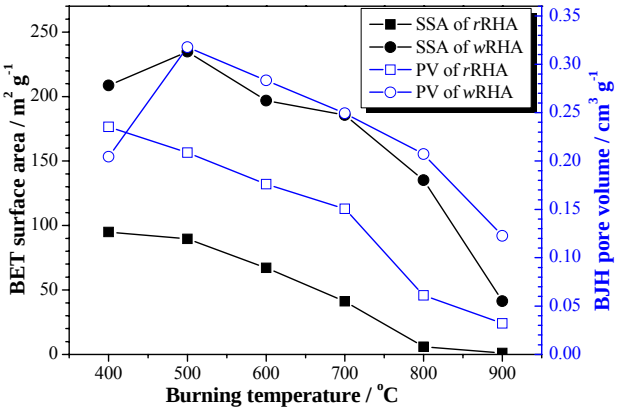

Figure 3. BET surface area (solid) and BJH pore volume (open) of *r*RHAs (square) and *w*RHAs (circle).

Conclusions

We carried out an investigation into the burning temperature dependence of the structure and physicochemical properties, such as surface and pore volume, of RHA. As to structure, the densification of the amorphous silica structure of the ashes becomes lower with the increase of T_b;

the Si−O−Si bond angle increases with T_b; the silica in *w*RHAs possesses a denser short-range order structure and the Si−O−Si bonds of smaller angle than those in *r*RHAs. As to physicochemical properties, the SSA and the PV of RHA decrease with T_b when solid combustibles are mostly burned off; the T_b dependence of SSA and PV is strongly related to the components of the ashes; at the same T_b *w*RHAs have a higher SSA and a larger PV than *r*RHAs. Such dependences are of particular interest in structure and property optimization of rice husk silica by T_b.

Acknowledgements

We thank Prof. J.-L Shi and A/P. L.-X. Zhang of SICCAS for the help in N_2-sorption experiments. This work was supported by the 'High-Tech Research Center' project for private universities from MEXT of Japan.

References

1. Agarwal, A., Davis, K. M. and Tomozawa, M. 1995. A simple IR spectroscopic method for determining fictive temperature of silica glasses. *J. Non-Cryst. Solids* **185(1-2)**: 191-198

2. Armesto, L., Bahillo, A., Veijonen, K., Cabanillas, A. and Otero, J. 2002. Combustion behaviour of rice husk in a bubbling fluidized bed. *Biomass Bioenergy* **23(3)**: 171-179.

3. Chandrasekhar, S., Satyanarayana, K.G., Pramada, P.N., Raghavan, P. and Gupta, T. N. 2003. Processing, properties and applications of reactive silica from rice husk—an overview. *J. Mater. Sci.* **38(15)**: 3159-3168.

4. Chang, F. W., Kuo, W. Y. and Yang, H. C. 2005. Preparation of Cr2O3-promoted copper catalysts on rice husk ash by incipient wetness impregnation. *Appl. Catal. A : Gen.* **288**: 53-61.

5. Feng, Q. G., Lin, Q. Y., Gong, F. Z., Sugita, S. and Shoya, M. 2004. Adsorption of lead and mercury by rice husk ash. *J. Colloid Interface Sci.* **278**: 1-8.

6. Shinohara, Y. and Kohyama, N. 2004. Quantitative analysis of tridymite and cristobalite crystallized in rice husk ash by heating. *Ind. Health* **42**: 277-285.

7. Sun, L and Gong, K. 2001. Silicon-based materials from rice husks and their applications. *Ind. Eng. Chem. Res.* **40**: 5861-5877.

8. Umeda, J. and Kondoh, K. 2008. Highly-purity amorphous silica originated in rice husks via carboxylic acid leaching process. *J. Mater. Sci.* **43(22)**: 7084-7090.

9. Wang, H. P., Lin, K. S., Huang, Y.J., Li, M.C. and Tsaur, L.K. 1998. Synthesis of zeolite ZSM-48 from rice husk ash. *J. Hazard. Mater.* **58**: 147-152.

10. Xiong, L., Saito, K., Sekiya, E. H., Sujaridworakun, P. and Wada, S. 2009. Influence of impurity ions on rice husk combustion. *RHAsia 2009: RH-O-22.*

11. Xiong, L., Saito, K, Wada, S. and Sekiya, E. H. 2009. Utilization of rice husk to synthesize high-performance phosphors. *RHAsia 2009: RH-O-24.*